Chinese Chemical Letters 33 (2022) 1545–1549

Contents lists available at ScienceDirect

Chinese Chemical Letters

journal homepage: www.elsevier.com/locate/cclet

Programmed co-assembly of DNA-peptide hybrid microdroplets by phase separation

Shengtao Yao[a], Yue Liao[a], Rizhao Pan[a], Weiping Zhu[a], Yufang Xu[a,*], Yangyang Yang[a,*], Xuhong Qian[a,b,*]

[a] School of Pharmacy, Shanghai Key Laboratory of Chemical Biology, East China University of Science and Technology, Shanghai 200237, China
[b] State Key Laboratory of Bioreactor Engineering, East China University of Science and Technology Shanghai 200237, China

ARTICLE INFO

Article history:
Received 2 July 2021
Revised 26 August 2021
Accepted 27 August 2021
Available online 2 September 2021

Keywords:
Self-assembly
Microdroplet
DNA origami
Phase separation
Elastin-like polypeptides

ABSTRACT

Biopolymers, including DNA and peptides have been used as excellent self-assembling building blocks for programmable single-component or hybrid materials, due to their controlled molecular interactions. However, combining two assembling principles of DNA-based programmability and peptide-based specific molecular interactions for hybrid structures to microscale has not yet been achieved. In this study, we describe a hybrid microsystem that emerges from the co-assembly of DNA origami structure and short elastin-like polypeptide conjugated oligonucleotides, and initiates liquid-liquid phase separation to generate microdroplets upon heating above the transition temperature. Moreover, the hybrid microdroplets are capable for guest molecule trapping and perform bi-/tri-enzymatic cascades with rate enhancements as open "microreactors". Our programmed assembled DNA-peptide microsystem represents a new combination of DNA nanotechnology and peptide science and opens potential application routes toward life-inspired biomaterials .

Nature uses self-assembly to build up materials with distinctive structures, length scales, physical and chemical properties and remarkable functions. Developing new self-assembly systems could facilitate the fabrication of smart materials with increased complexity and life-inspired functionality, in which building block design plays essentials roles in determining the self-assembly process and controlling the structural length scale [1–3]. Therefore, DNAs or peptides are highly favored bioinspired self-assembling polymers due to their controlled intermolecular interactions. Sequence-specific DNA duplex recognition has been intensively studied for two- and three-dimensional nanostructures (2D- and 3D-nanostructures), colloids, and hydrogels [4]. Peptides with specific folding patterns and functions could be designed *de novo* and assembled into structures such as mimicking proteins and protein microparticles [5,6]. In addition, with the involvement of DNA-based assembling and peptide-specific interactions, the coassembly of DNAs and peptides allows the increase in complexity, resulting in hybrid structures, including micelles, vehicles, and nanofibers [7,8]. In contrast, producing such self-assembly hybrids on a macrostructural scale with combined assembling principles remains challenging. Recently, phase separation has become an important strategy for producing DNA-based micron- and nano-sized particles. Walther *et al.* developed all-DNA colloids and ATP-fueled DNA coacervates, using long linear DNA structures [9,10]. Moreover, limited-valence DNA nanostars have been thoroughly used to produce microdroplets *via* liquid-liquid phase separation (LLPS) [11,12]. Wilks *et al.* developed poly(NIPAM)-decorated DNA-tetrahedron and generated nano-sized coacervate at 40 °C [13]. However, the phase separation-based formation of DNA- and peptide-containing hybrid assemblies has not yet been reported. DNA origami method, using a long single-stranded DNA and over 200 staple strands not only allows the production of nanostructures in desired shapes but also provides more than 100 addressable sites to integrate with guest molecules [14]. DNA origami structures have been demonstrated as smart materials with applications in various fields, including nanorobotics [15], biomedicine [16], nanophotonics [17,18] and single-molecule analysis [19]. Several studies reported the application of DNA origami structures to integrate with peptides for producing coassembled hybrid structures in ordered nanopatterns, demonstrating that DNA origami structures are excellent multivalent nanoscaffolds for accumulating peptides and allowing more complex peptide interactions [20–22]. However, the expansion of the length scale of such hybrids from a nanoscale to microscale has not yet been achieved. Elastin-like

* Corresponding authors.
E-mail addresses: yfxu@ecust.edu.cn (Y. Xu), triyang@ecust.edu.cn (Y. Yang), xhqian@ecust.edu.cn (X. Qian).

https://doi.org/10.1016/j.cclet.2021.08.116
1001-8417/

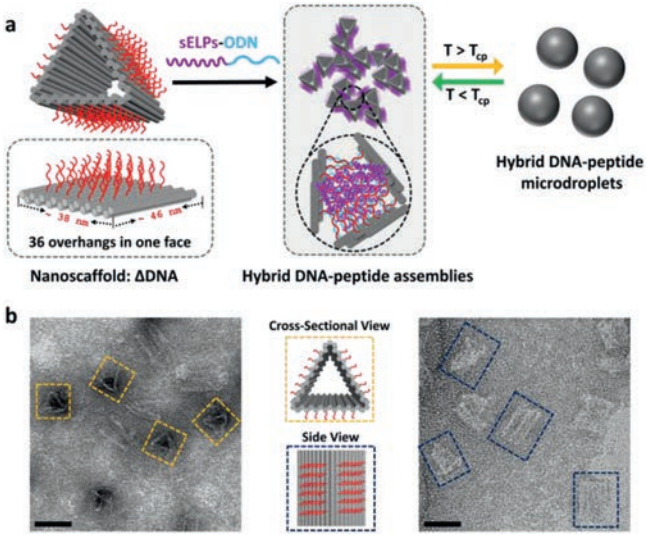

Fig. 1. (a) Schematic drawings of self-assembly hybrid microdroplets composed of DNA and peptide by programmed co-assembly of DNA origami structure with short elastin-like polypeptides conjugated oligonucleotides and induced phase separation upon heating above transition temperature. (b) TEM images of ΔDNA from cross-sectional view (left) and side view (right). Scale bars: 40 nm.

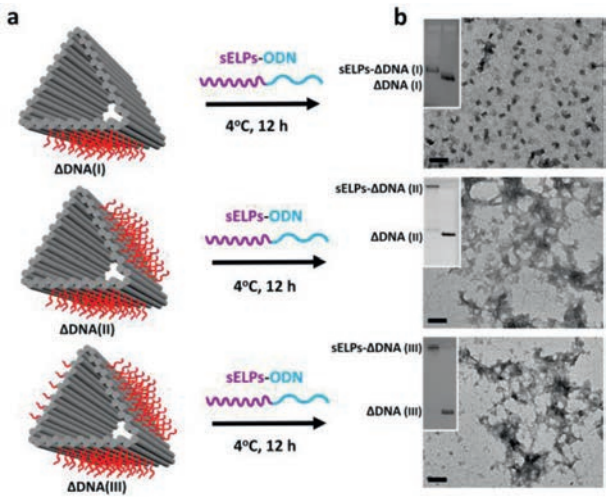

Fig. 2. (a) Programmed co-assembly of ΔDNAs with sELPs-ODN to form the hybrid assemblies at 4 °C for 12 h, which were confirmed by (b) using AGE analysis (0.9%) (inset images) and TEM imaging. Scale bars: 100 nm.

polypeptides (ELPs), composed of repeated pentapeptide units of $(Val\text{-}Pro\text{-}Gly\text{-}Xaa\text{-}Gly)_N$ (VPGXG, N is the number of repeated units and X can be any amino acid except proline), are well-known to exhibit lower critical solution temperature (LCST)-like phase separation behaviors and have been widely studied to produce nanostructures or hydrogels [23,24]. However, the synthetic short ELPs (sELPs) are less explored due to their intrinsic high transition temperatures (T_t). Despite this, continuous efforts have still been made to investigate the expansion of sELPs functional applications, due to the ease of their synthesis. The covalent conjugation of sELPs with peptides or oligonucleotides has been demonstrated as useful approach to regulate the hydrophobic domains and has been applied for the programmed assembly of nanoscale objects [25,26].

To this end, we developed a programmed coassembly hybrid system by emerging the DNA origami structures and sELPs and then performed phase separation to form microdroplets upon heating above T_t. A DNA origami structure containing over 100 overhangs on outer surfaces is used as an assembly scaffold to accumulate sELPs (only 6 pentapeptide repeats) conjugated oligonucleotides (sELPs-ODN) (Fig. 1). Moreover, the hybrid microdroplets are demonstrated to generate functions including guest molecules trapping and perform enzymatic cascade reactions with rate enhancement.

The DNA origami structure was rationally designed in a triangular prism shape (ΔDNA, *ca.* 46 nm × 38 nm × 38 nm) for the following reasons (Fig. 1a, Fig. S1 in Supporting information): (1) Each ΔDNA contains more than 100 staple strands, indicating that much more sELPs could be concentrated on a structure surface with numeric and positional control; (2) the hollow prism structure consists of single-layered dsDNA, is semi-rigid, and allows more complex interactions of anchored sELPs; and (3) the triangular prism shape provides the structural support and richer three-dimensionality for sELPs. In the original design, each outer face of ΔDNA was designed with 36 single-stranded oligonucleotides (5′-TCTCTTCACCGTAATCTT-3′, same sequences) as overhangs (ss-overhangs), which offers a total of 108 anchoring sites for sELPs. The sELPs-ODN were synthesized by conjugating 5′ terminal azido-tethered oligonucleotide (N_3-ODN) with alkyne-tethered sELPs ($[VPGFG]_6$, 30 amino acids, Table S1 in Supporting information) in water/dimethyl sulfoxide-mixed solvent *via* a copper(I)-catalyzed azide-alkyne cycloaddition reaction (Fig. S2 in Supporting information). The conjugates were confirmed by denatured polyacrylamide gel electrophoresis (PAGE), the ratio change in $\lambda_{abs}260$ nm/$\lambda_{abs}230$ nm and LC-MS (Figs. S2 and S3 in Supporting information). ΔDNA was prepared in a one-pot reaction: 200 oligonucleotide staple strands (5 equiv.) and the M13mp18 scaffold (7249 nt) were self-assembled into the designed structure during a three-step annealing process. Then the samples were purified four times by centrifuge filters to completely remove extra staples. The purified ΔDNA was confirmed by agarose gel electrophoresis (AGE, 0.9%) (Fig. S4a in Supporting information) and transmission electron microscopy (TEM) (Fig. 1b, Fig. S4b in Supporting information). It is observed that ΔDNAs were successfully constructed and most of them were slightly distorted (in a cross-sectional view and side view images), indicating the semi-rigidness characteristic.

The coassembly of sELPs-ODN and ΔDNA were performed in three different models (Fig. 2a): ΔDNA(I), with 36 overhangs on 1 face, ΔDNA(II), with 72 overhangs on 2 faces, and ΔDNA(III), with 108 overhangs on 3 faces hybridized with sELPs-ODN in 3 equivalent ratios: 1:36, 1:72 and 1:108 (ΔDNA:sELPs-ODN), respectively. The assembled products were then analyzed by AGE (0.9%) and TEM (Fig. 2b, Fig. S5 in Supporting information). As shown in Fig. 2b, most sELPs-ΔDNA(I) were slightly folded but remained dispersed in a nanostructural formation. Previously Pirzer *et al.* reported a dynamic rectangular DNA origami structures, which showed reversible intrastructural folding behaviors by utilizing phase-transition performances of ELPs($(GVGVP)_{40}$) [27]. Here, the hybrid structure of sELPs-ΔDNA(I) showed similar intrastructural folding when one face of ΔDNA(I) was anchored with 36 sELPs due to the enhanced hydrophobic interactions (Fig. S6 in Supporting information). In AGE images, the band of sELPs-ΔDNA(I) showed a slower migration rate than ΔDNA(I). For sELPs-ΔDNA(II) and sELPs-ΔDNA(III), the bands on AGE images both showed almost no migration, indicating that large structures might be formed. In TEM images, the dispersed nanostructures were merely observed but aggregate-like disordered structures were shown instead, indicating more complex interactions between intra- and inter-interactions of sELPs on the surface of ΔDNA. These results demonstrated that sELPs-ODN were successfully assembled onto three ΔDNAs and exhibited increased hydrophobic interactions on the DNA origami structures with sELPs increase. To further investigate the advantage of ΔDNA, we also prepared a 2D hexagonal-shaped DNA nanostructure (HEX-DNA) [28], and introduced a to-

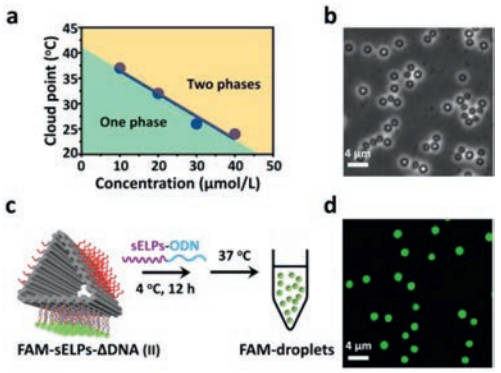

Fig. 3. (a) Evolution of cloud point temperature (T_{cp}) as a function of concentration of sELPs-ΔDNA(III) (The concentration of sELPs-ΔDNA means the concentrated ELPs in hybrid assemblies.). (b) Morphology of sELPs-ΔDNA(III) at 37 °C in DIC microscopy. (c) Construction of FAM-droplets and (d) CLSM image excited at 488 nm.

tal of 114 sELPs onto surface (Figs. S7 and S8 in Supporting information). However, no aggregate-like disordered structures were imaged by TEM but all monodispersed nanostructures (Fig. S9 in Supporting information), indicating that ΔDNA offers richer interactions of sELPs than HEX-DNA.

For recombinant long ELPs, it has been extensively characterized that concentration is an important factor for LCST phase behaviors [29]. Since one-faced hybrid assemblies remained in dispersed nanostructures, here we focused on the investigation of the phase-separation behaviors of disordered hybrid assemblies of sELPs-ΔDNA(II) and sELPs-ΔDNA(III). Fig. 3a demonstrated that sELPs-ΔDNA(III) exhibited concentration-dependent LCST phase behaviors (Fig. S10 in Supporting information). The cloud point temperature decreased with increasing sELPs-ΔDNA(III) concentration ($T_{cp} \approx 32$ °C, 20 μmol/L). Then morphology of sELPs-ΔDNA(III) after phase separation was examined next. After the heating treatment of sELPs-ΔDNA(III) at 37 °C (higher than T_t), the sample was imaged under differential interference contrast (DIC) microscopy and scanning electron microscope (SEM). As shown in Fig. 3b, Figs. S11 and S12 (in Supporting information), spheroidal and uniform droplets in a diameter of ~1.2 μm were observed. Then we investigated dynamic phase behaviors by real-time observation of the formation of microdroplets. After loading the assembled products to the observation chamber preheated to 37 °C, the phase transition was initiated. In Fig. S13 (Supporting information), the time-lapsed images demonstrated that hybrid microdroplets were formed in tens of seconds. For sELPs-ΔDNA(II), similar phase separation behaviors and dynamic microdroplet formation process were also successfully observed (Figs. S14 and S15 in Supporting information) but no microdroplets were observed of sELPs-HEX-DNA assemblies (Fig. S16 in Supporting information). Besides, fluorescence recovery after photobleaching (FRAP) experiments (Fig. S17 in Supporting information) showed that the fluorescence of nile red in microdroplets was efficiently recovered in tens of seconds, indicating the liquid-like property of droplets. Furthermore, we used TEM imaging to confirm the structure of hybrid assemblies by decreasing the solution temperature of hybrid microdroplets to 4 °C, which showed that the aggregate-like disordered structures were observed again, indicating the reversible and controllable process of our hybrid microsystem (Fig. S18 in Supporting information). Here short ELPs were programmed assembled onto ΔDNA, resulting the enhanced hydrophobic interactions of ELPs in confined nanospace, which probably made the contribution to the phase separation of hybrid assemblies.

To facilitate observation and verify that microdroplets are hybrids composed of ΔDNA and sELPs, a fluorescent-labeling strategy was introduced into sELPs-ΔDNA(II), in which 36 overhangs on 1 face are replaced to hybridize with carboxyfluorescein (FAM)-labeled single-stranded DNA (FAM-ssDNA) (Fig. 3c). After assembly preparation and heat treatment, the FAM-sELPs-ΔDNA(II) was directly observed by using confocal laser scanning microscopy (CLSM). Uniform fluorescent droplets (FAM-droplets) were clearly imaged, indicating that the droplets were composed of sELPs and ΔDNA (Fig. 3d, Fig. S19 in Supporting information). The reversible droplet formation was confirmed by regulating temperature at 4, 37 and 4 °C continuously (Fig. S20 in Supporting information). Under CLMS, no droplets were observed at 4 °C initially. After increasing to 37 °C, fluorescent microdroplets were clearly imaged. By decreasing back to 4 °C, the microdroplets disappeared again. These results illustrated that both the hybrid assemblies of sELPs-ΔDNA(II) and sELPs-ΔDNA(III) could undergo phase separation to form microdroplets when heated above T_t and the process was reversible and controlled.

For proof-of-concept applications, we examined the potentials of our hybrid microsystem as open "microreactor". First, we evaluated the ability of sELPs-ΔDNA microdroplets to organize guest molecules in a droplet state due to the lack of physical membrane. As shown in Fig. 4a, FAM-sELPs-ΔDNA(II) containing free ss-overhangs, was prepared and incubated at 37 °C to form FAM-droplets, then TAMRA-ssDNA complementary to free ss-overhangs was added and incubated at 37 °C for another 5 min. From the optical images shown in Fig. 4b and Fig. S21 (Supporting information), TAMARA-ssDNA could diffuse into FAM-droplets and be sequestered inside upon hybridization. Therefore, the hybrid microdroplets showed permeability and guest molecules could be sequestered by microdroplets. Moreover, our hybrid microsystem could undergo phase separation at physiological temperature, which might be suitable for bio-related and cellular mimic applications. First, we introduced a cascade biocatalytic reaction model: glucose oxidase/horseradish peroxidase (GOx/HRP) [30] into hybrid microsystem. ΔDNA(II), tethering GOx or HRP, was prepared (Fig. S22 in Supporting information); then, sELPs-ODN were introduced into the GOx-ΔDNA(II) and HRP-ΔDNA(II) solution, separately. The solution of GOx-sELPs-ΔDNA(II) and HRP-sELPs-ΔDNA(II) were mixed at 4 °C and heated to 37 °C to form hybrid microdroplets (GOx/HRP droplets) (Fig. S23 in Supporting information). Glucose can freely go through microdroplets and be oxidized by GOx to generate H_2O_2, which is subsequently involved with HRP to mediate the oxidation of 2′,2′-azino-bis(3-ethylbenzthiazoline-6-sulphonic acid), $ABTS^{2-}$, resulting in the colored product, $ABTS^{-\bullet}$ ($\lambda_{abs} = 414$ nm) (Fig. 4c). The cascade enzymatic reactions in microdroplets were examined by evaluating the formation of $ABTS^{-\bullet}$ at 37 °C. In Fig. 4d, the black curve showed the time-dependent formation of $ABTS^{-\bullet}$ when GOx/HRP pair in microdroplets (37 °C), the blue curve indicated the accumulation of $ABTS^{-\bullet}$ when GOx-sELPs-ΔDNA(III) and HRP-sELPs-ΔDNA(III) were in a disperse state (no droplet, 25 °C) and the red curve depicted the rate of $ABTS^{-\bullet}$ generation in ssDNA conjugated enzyme solution (37 °C), in which the enzyme concentrations were monitored carefully to maintain consistency. We found that that the catalytic rates was enhanced in the microdroplets as compared to ssDNA-enzyme solution owing to the combined effect of molecular crowding and reduced diffusional barrier of chemicals in crowded microenvironments, which corresponded with GOx/HRP cascade reactions in DNA coacervates developed by Walther *et al.* as well as other coacervate-based protocell models [31]. To evaluate whether phase transition of hybrid microsystem could affect the cascade reaction rate, we performed the cascade reactions in GOx/HRP-droplets by switching the reaction temperature at 25 °C (lower than T_t, dispersed state) and 37 °C (higher than T_t, microdroplet state), separately. We first confirmed that these two reaction temperatures had less effect on the catalytic rates (Fig. S24 in Supporting information).

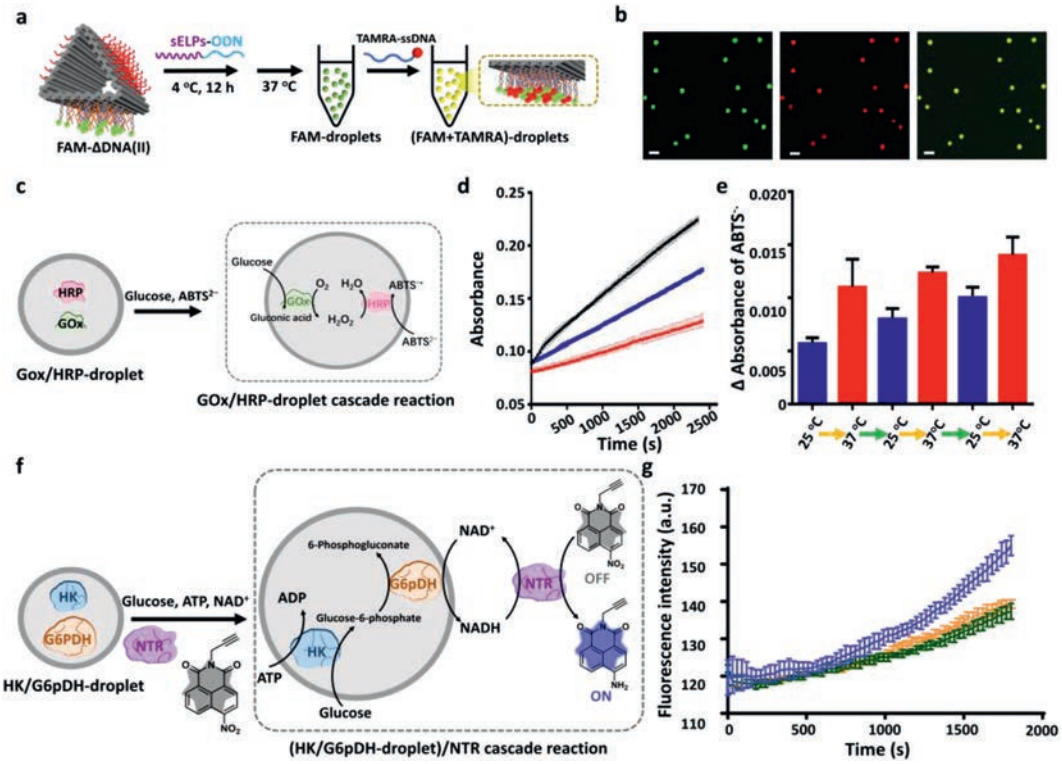

Fig. 4. Evaluation of guest molecule capturing and performing cascade biocatalytic reactions of hybrid microsystem. (a) Schematic drawings of concentrating TAMRA-ssDNA into FAM-droplets by the hybridization of TAMRA-ssDNA with the free overhangs on ΔDNA. (b) CLMS and merged images of TAMRA/FAM-droplets excited at 488 nm, 561 nm, respectively. Scale bars: 3 μm. (c) A cascade reaction model: GOx/HRP pair was introduced into hybrid microdroplets. Glucose can free penetrate into GOx/HRP-droplet and initiates the cascade catalytic reaction, generating the colored product $ABTS^{\bullet-}$. (d) Time-dependent absorbance changes at 414 nm as a result of the oxidation of $ABTS^{2-}$ by cascade reaction in GOx/HRP droplets (37 °C, black curve), in GOx/HRP sELPs-ΔDNA(III) (25 °C, blue curve) and in bulk solution containing free ssDNA-enzyme pair (25 °C, red curve), respectively. (e) Continuous and regulatory cycles of GOx/HRP modified hybrid microsystem at 25 °C and 37 °C, separately. (f) Design of (HK/G6pDH-droplet)/NTR redox reaction in hybrid microsystem: glucose is phosphorated to glucose-6-phosphorate by HK in the presence of ATP, which is further converted to 6-phosphogluconate together with the generation of NADH. A fluorescent probe of NTR (NTR-probe, fluorescence off) is reduced to fluorescence-on molecule containing amino group by NTR by oxidizing NADH to NAD^+. (g) Time-dependent fluorescence change (off to on) of NTR-probe at two temperatures of 37 °C (purple curve) and 25 °C (orange curve), and in bulk solution containing free ssDNA-enzyme cascades (37 °C, green curve), respectively.

Then the absorbance changes (ΔAbs) indicating the new formed $ABTS^{\bullet-}$ in 240 s are recorded in Fig. 4e and showed slower catalytic rate at 25 °C and faster catalytic rate at 37 °C owing to the phase separation of hybrid assemblies between dispersed state and droplet state. Moreover, another two continuous reaction cycles at 25 °C and 37 °C were performed, resulting repeated increased and decreased product of $ABTS^{\bullet-}$ between two states, which demonstrated the reversible controllability of our hybrid microsystem (Fig. 4e). Next, we utilized the hybrid microsystem to mimic cellular redox reactions by employing hexokinase (HK) and glucose-6-phosphate dehydrogenase (G6pDH). HK/G6pDH catalytic pair are major cascade enzymes participating intracellular aerobic glycolysis, in which HK catalyzed glucose to glucose-6-phosphate, and G6pDH oxidized glucose-6-phosphate by simultaneously reducing nicotinamide adenine dinucleotide (NAD^+) to NADH [32,33]. On other hand, nitroreductase (NTR) is a key biomarker of hypoxia and can reduce nitroaromatic derivatives to amines by using NADH as an electron donor [34–38]. Here NTR is combined with HK/G6pDH pair to become a tri-enzymatic redox reaction model (Fig. 4f). A fluorescent probe (NTR-probe) (Figs. S25–S27 in Supporting information) was synthesized and reduced by NTR in the presence of NADH generated by HK/G6pDH pair, inducing a fluorescence off-to-on response of 1,8-naphthalimide (λ_{em} = 550 nm) [39]. HK/G6pDH droplets were prepared same as GOx/HRP-droplets (Figs. S23 and S28 in Supporting information) and reactants including glucose, ATP, NAD^+ and NTR were added into the HK/G6pDH-droplet solution to initiate the redox reaction. The time-dependent fluorescence changes of NTR-probe at three different conditions were shown in Fig. 4g. We find that the fluorescence of NTR-probe in the hybrid microsystem (37 °C, purple curve) was gradually increased, demonstrating that this cascade redox reactions were successfully performed in microsystem and catalytic rate was also enhanced comparing to either dipersed catalytic system (25 °C, orange curve) or free ssDNA-enzymatic cascades in bulk solution (37 °C, green curve). Furthermore, the time-dependent fluorescence increasement of NTR probe in microdroplets was observed by using CLSM (Fig. S29 in Supporting information). Therefore, our hybrid microdroplets could not only trap functional molecules but also be recognized as open "microreactor" with compatibility of biocatalytic reactions.

In summary, we successfully developed a programmed assembly hybrid microsystem by combining two orthogonal biomoelcular assembling principles. ΔDNA, a 3-dimensional DNA origami nanostructure, containing 36 overhangs on each outer face was rationally constructed and used as a scaffold to assemble with sELPs-ODN. By precisely controlling the amount of sELPs on the ΔDNA, two hybrid assembly structural morphorlogies were obtained, including slightly folded hybrid nanostructure, when one ΔDNA face was loaded with sELPs, just as well as aggregate-like disordered large structures, when two or three ourter faces were occupied, demonstrating that the concentrated sELPs hydrophobicity was enhanced with increase in sELPs on the ΔDNA. Moreover, the hybrid assemblies, containing 72 sELPs (2-face assembling) and 108 sELPs (3-face assembling) on each DNA origami structure exhibited LLPS behaviors and formed uniform liquid-like microdroplets when heated above T_t. The process was reversible and controlled, and we

directly visualized it under bright-field microscopy. Finally, our hybrid microdroplets showed the capacity to capture guest molecules and perform biocatalytic cascade reactions with enhanced catalytic rates. Overall, our hybrid microdroplet system combines DNA nanotechnology with peptide science, which not only expands the potential applications of DNA or peptide-based biomaterials, especially DNA origami structures, but also opens new routes toward life-inspired materials.

Declaration of competing interest

The authors declare that they have no known competing financial interests or personal relationships that could have appeared to influence the work reported in this paper.

Acknowledgment

This work was supported by the National Natural Science Foundation of China (No. 31600802).

Supplementary materials

Supplementary material associated with this article can be found, in the online version, at doi:10.1016/j.cclet.2021.08.116.

References

[1] F. Hong, F. Zhang, Y. Liu, H. Yan, Chem. Rev. 117 (2017) 12584–12640.
[2] D.M. Raymond, B.L. Nilsson, Chem. Soc. Rev. 47 (2018) 3659–3720.
[3] T. MacCulloch, A. Buchberger, N. Stephanopoulos, Org. Biomol. Chem. 17 (2019) 1668–1682.
[4] Y.H. Dong, C. Yao, Y. Zhu, et al., Chem. Rev. 120 (2020) 9420–9481.
[5] E. Michel, A. Pluckthun, O. Zerbe, Angew. Chem. Int. Ed. 57 (2018) 4576–4579.
[6] Y.M. Wong, H. Masunaga, J.A. Chuah, et al., Biomacromolecules 17 (2016) 3375–3385.
[7] M. Kye, Y.B. Lim, Angew. Chem. Int. Ed. 55 (2016) 12003–12007.
[8] M. Humenik, T. Scheibel, ACS Nano 8 (2014) 1342–1349.
[9] R. Merindol, S. Loescher, A. Samanta, A. Walther, Nat. Nanotechnol. 13 (2018) 730–738.
[10] J. Deng, A. Walther, Chem 6 (2020) 3329–3343.
[11] B.J. Jeon, D.T. Nguyen, O.A. Saleh, J. Phys. Chem. B 124 (2020) 8888–8895.
[12] Y. Sato, T. Sakamoto, M. Takinoue, Sci. Adv. 6 (2020) eaba3471.
[13] T.R. Wilks, J. Bath, J.W. de Vries, et al., ACS Nano 7 (2013) 8561–8572.
[14] P.W.K. Rothemund, Nature 440 (2006) 297–302.
[15] F. Wang, X.Q. Liu, I. Willner, Angew. Chem. Int. Ed. 54 (2015) 1098–1129.
[16] Q. Jiang, C. Song, J. Nangreave, et al., J. Am. Chem. Soc. 134 (2012) 13396–13403.
[17] S. Gwo, H.Y. Chen, M.H. Lin, et al., Chem. Soc. Rev. 45 (2016) 5672–5716.
[18] H. Yu, T.T. Man, W. Ji, et al., Chin. Chem. Lett. 30 (2019) 175–178.
[19] S. Hernandez-Ainsa, U.F. Keyser, Nanoscale 6 (2014) 14121–14132.
[20] J. Jin, E.G. Baker, C.W. Wood, et al., ACS Nano 13 (2019) 9927–9935.
[21] A. Buchberger, C.R. Simmons, N.E. Fahmi, et al., J. Am. Chem. Soc. 142 (2020) 1406–1416.
[22] T. Jiang, T.A. Meyer, C. Modlin, et al., J. Am. Chem. Soc. 139 (2017) 14025–14028.
[23] S. Roberts, M. Dzuricky, A. Chilkoti, FEBS Lett. 589 (2015) 2477–2486.
[24] H. Zhao, V. Ibrahimova, E. Garanger, S. Lecommandoux, Angew. Chem. Int. Ed. 59 (2020) 11028–11036.
[25] J.Y. Qin, J.D. Sloppy, K.L. Kiick, Sci. Adv. 6 (2020) eabd3033.
[26] B. Wang, R.Z. Pan, W.P. Zhu, et al., Soft Matter 17 (2021) 1184–1188.
[27] M.A. Goetzfried, K. Vogele, A. Muckl, et al., Small 15 (2019) 1903541.
[28] Y.Y. Yang, S.W. Zhang, S.T. Yao, et al., Chem. Eur. J. 25 (2019) 5158–5162.
[29] J.R. McDaniel, D.C. Radford, A. Chilkoti, Biomacromolecules 14 (2013) 2866–2872.
[30] X.M. Sun, Y. Li, Q. Yang, et al., Chin. Chem. Lett. 32 (2021) 1780–1784.
[31] J.B. Li, X.M. Liu, L.K.E.A. Abdelmohsen, et al., Small 15 (2019) 1902893.
[32] P. Heneberg, Antioxid. Redox Sign. 30 (2019) 415–442.
[33] S.Y. Lunt, M.G. Vander Heiden, Annu. Rev. Cell Dev. Bi. 27 (2011) 441–464.
[34] G.L. Ke, M.H. Liu, S.X. Jiang, et al., Angew. Chem. Int. Ed. 55 (2016) 7483–7486.
[35] Y.H.R. Yang, J.L. Fu, S. Wootten, et al., ChemBioChem 19 (2018) 212–216.
[36] Y.H. Chen, G.L. Ke, Y.L. Ma, et al., J. Am. Chem. Soc. 140 (2018) 8990–8996.
[37] J. Chen, R.J. Dai, B. Tong, S.Y. Xiao, W.W. Meng, Chin. Chem. Lett. 18 (2007) 10–12.
[38] W.J. Qin, C.C. Xu, Y.F. Zhao, et al., Chin. Chem. Lett. 29 (2018) 1451–1455.
[39] J. Zhou, W. Shi, L.H. Li, et al., Chem. Asian J. 11 (2016) 2719–2724.